



Seismic performance of a nonhomogeneous slope reinforced by anchored piles using centrifuge tests

Tong Zheng^{1,2} · Qiangqiang Sun³ · Hongshuai Liu³ · Wenhao Qi^{1,2} · Rui Sun^{1,2}

Received: 26 November 2021 / Accepted: 21 January 2024 / Published online: 30 January 2024
© The Author(s) 2024

Abstract

This paper conducts a series of centrifuge model tests to evaluate the seismic response characteristics of an anchor-pile-slope system. A real reinforced nonhomogeneous slope that remained stable during the 2008 Wenchuan earthquakes is utilized as the reference prototype. The recorded ground motion near the slope is selected as the seismic input. The responses in terms of slope acceleration and deformation, earth pressure, pile deformation and bending moment, and the anchor cable axial force are measured. The results have demonstrated that the slope vertical settlements and pile head displacements increase with increasing motion intensity. The maximum acceleration amplification is observed around the pile head, and the accelerations around the bedrock surface are attenuated. The largest dynamic earth pressure occurs at the pile head and then decreases with increasing depth due to the decreased soil-pile relative deformation. The presence of the anchor cable inhibits the build-up of dynamic earth pressure and leads to a negative bending moment. The maximum bending moment appears around the soil-rock interface because of the significant stiffness difference. Experimental results also illustrate that the axial force of the anchor cable is proportional to the pile head deformation. This work provides experimental evidence on the seismic behavior of a slope reinforced by anchored piles and will be beneficial to the calibration of numerical models and design methods.

Keywords Centrifuge model · Slope · Wenchuan earthquake · Anchored piles

Introduction

The seismic response of slopes in earthquake-prone areas arises much concern in design since the unfavorable seismic forces would lead to slope instability. The landslide caused by earthquakes is one of the major geo-disasters in the whole world, resulting in serious consequences in past and recent earthquakes (Huang et al. 2017; Huang and Li 2009; Kawashima et al. 2010; Keefer 1984; Sharma and Deng 2019; Shrestha and Kang 2019; Tsai et al. 2018; Wartman et al. 2013). Although some slopes remained stable during

the earthquake event, the slopes were locally cracked, hence increasing the potential risk of instability during rainfall, traffic loading, and other adverse conditions (Al-Defae et al. 2013; Keefer 1994; Song et al. 2012; Tang et al. 2011; Yang et al. 2021; Yin et al. 2015). Consequently, it is an important issue to improve slope stability before and after earthquakes.

Different reinforcement techniques have been developed to prevent seismic-induced displacement (Bi et al. 2019; Kang et al. 2009; Usluogullari et al. 2016; Ye et al. 2019; Zhang et al. 2020). The choice of an appropriate reinforcement technique should be consistent with the size of the possible landslides, the definition of seismic forces, as well as the budget. For preliminary design stages, stabilizing piles is a commonly utilized method. More recently, a new type of slope reinforcement technique named anchored pile has received increasing attention. It is believed that the additional use of an anchor cable allows for modifying the stress and deformation in a slope and will improve the workability of the reinforced pile. By utilizing an anchor, it is possible to produce smaller internal forces and deformations of a pile. As a result, the number and the size of piles decrease.

✉ Qiangqiang Sun
sun_ease@126.com

¹ Key Laboratory of Earthquake Engineering and Engineering Vibration, Institute of Engineering Mechanics, China Earthquake Administration, Harbin 150080, China

² Key Laboratory of Earthquake Disaster Mitigation, Ministry of Emergency Management, Harbin 150080, China

³ Institute of Geotechnical Engineering, Hebei University, Baoding, China

Therefore, the anchored pile is an economical and practical technique, as stated in the literature (Kang et al. 2009; Siller et al. 1991; Song et al. 2012). Qu et al. (2018) performed a shaking table test to investigate the seismic response characteristic of an anchored sheet pile wall, considering uniform backfill soil. Based on centrifuge modeling tests, Huang et al. (2020a) studied the evolution of internal forces in terms of the pile bending moment and shear force, the anchor axial force during the progressive slide of a slope. They found that the presence of an anchor could modify the failure mode of the slope. The factor of safety and the permanent displacement of a reinforced slope were analyzed numerically by Huang et al. (2020b). They concluded that the utilization of an anchor-pile structure would significantly reduce the probability of failure. Pai and Wu (2021) carried out a shaking table test on a soil slope model reinforced by multi-anchor piles. They found that the anchor cable in combination with the energy dissipation spring could effectively reduce the acceleration responses in the slope body behind piles. On the other hand, historical earthquakes have demonstrated that the slope reinforced by anchored piles showed better seismic performance. For example, Liu et al. (2016) and Zhang et al. (2020) reported some slopes reinforced using this technique remained stable during earthquakes, although the recorded accelerations were much higher than the design acceleration.

In the framework of pseudo-static, simplified design methods enable to assessment of the transient changes in internal forces in pile and anchor during shaking. For such methods, the amplitude and distribution of acceleration responses should be precisely determined. On the other hand, experimental and numerical evidence of the permanent changes in the internal forces in the reinforced structures and deformation of a slope has emphasized that a full dynamic time-history analysis including soil-structure interaction and non-linear soil behavior should be conducted to achieve the most reliable seismic design of an anchor-pile-slope system. When a sophisticated numerical model exists, the accuracy of the numerical analysis of an anchor-pile-slope system needs to be verified. Due to the lack of well-documented full-scale case histories, it is difficult to validate any given design methods and numerical models, and hence, a centrifuge study is necessary. Since the available centrifuge study is very limited, some important issues are still unclear. In fact, due to the pronounced topographic effect and soil-structure interaction, the acceleration response should be very complicated under real ground motions, in comparison with that of an unreinforced homogeneous slope (Brennan and Madabhushi 2009).

Considering all the previous statements, the objective of this study is to evaluate the seismic response characteristics of an anchor-pile-slope system using centrifuge dynamic tests. A real reinforced nonhomogeneous slope that remained stable during the 2008 Wenchuan earthquakes is utilized as the reference prototype. The recorded ground

motion is scaled to four *PGAs* and is inputted to the model slope accounting for influences of earthquake sequences. The responses in terms of slope acceleration and deformation, dynamic earth pressure, pile deformation and bending moment, and the axial force of the anchor cable are measured and discussed. This work will not only provide new experimental evidence for the effectiveness of anchored pile reinforcement of a slope but also address several limitations of existing centrifuge dynamic tests.

Geological background

The slope studied is located in the Hanyuan, a county of Ya'an City. During the 2008 Wenchuan earthquake, this county suffered severe damages including massive building collapse and landslides (Yin et al. 2009). The seismic intensity of this county was up to VIII degree, with an estimated peak ground acceleration (*PGA*) of 0.38 g, much higher than the fortification intensity of VI degree corresponding to $PGA = 0.05$ g (Liu et al. 2016). The high acceleration amplitude could be attributed to the significant amplification effect caused by site conditions (Liu et al. 2016).

Despite high ground acceleration recorded, the Beihoushan ancient landslide group (located on the west of Hanyuan County) remained stable during shaking with only three tension cracks. The boundary of the landslide group was in the shape of an armchair with clear wings and a trailing edge, as illustrated in Fig. 1. Before the earthquake event, two reinforcement projects utilizing the technique of anchored piles were conducted to improve the stability of this landslide group. In the present study, landslide I is chosen as the reference prototype. This landslide is larger, with a length of about 30 m and a height of about 25 m. In

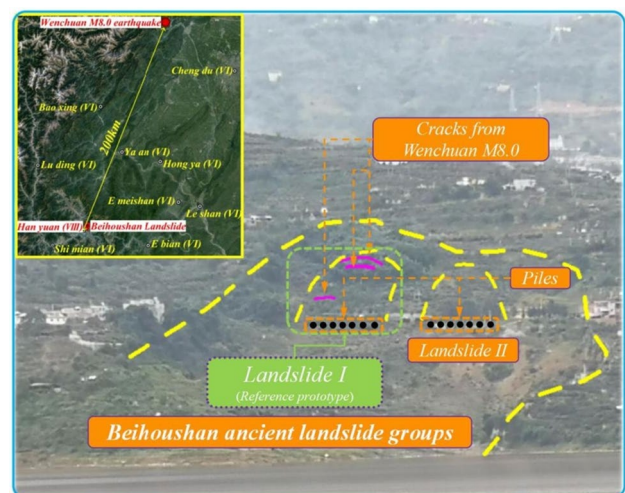


Fig. 1 Location of the Beihoushan ancient landslide group

addition, detailed design information about this landslide is available, including the design parameters of the piles and the morphology of the bedrock surface, which can guide the model design.

Based on the geological survey, the overlying soil is composed of yellowish-brown silty clay with varying thickness, while the underlying bedrock is the Xigeda formation (N_2x) mudstone (Fig. 2a). The shape of the bedrock surface presents a trifold line with dips respectively of 54° , 35° , and 11° from the top of the surface to the bottom. Seven concrete piles were arranged in a row, and the cross-section of the piles was rectangular with a size of $2.0\text{ m} \times 1.5\text{ m}$, with a length of 14 m (Fig. 2b).

Dynamic centrifuge tests

Test equipment

The dynamic centrifuge tests were carried out in the ZJU-400 large-scale geotechnical centrifuge at Zhejiang University (Fig. 3a). It consists of an electro-hydraulic

servo-hydraulic driving shaking table, with a maximum centrifugal acceleration of 150 g and a maximum capacity of 400 gt . The centrifuge has an effective rotation radius of about 4.5 m , which rotates about a central vertical axis.

The dimension of this high-performance shaking table is $800\text{ mm} \times 600\text{ mm}$ (Fig. 3b). In the case of the maximum weight of 500 kg , it can provide a maximum vibration amplitude of 40 g at a maximum centrifugal acceleration of 100 g . The shaking table can generate the sinusoidal wave and real earthquake wave with different amplitudes, frequencies, and duration times at the table bottom.

A model container with a Perspex viewing window was used in the centrifuge tests. The utilization of this type of box enabled the slope deformations and cracks through the Perspex window to be observed and filmed by a fast digital camera and video. The model box was made of an aluminum alloy and had inside dimensions of $600\text{ mm} \times 400\text{ mm} \times 500\text{ mm}$ (length \times width \times height). Concerning the box used in this research, DUXSEAL, a plastic, putty-like material that has a large damping ratio was applied to minimize the boundary effect on the slope model. The effectiveness of DUXSEAL as an absorbing

Fig. 2 Details of the studied slope: a site condition and b anchored piles

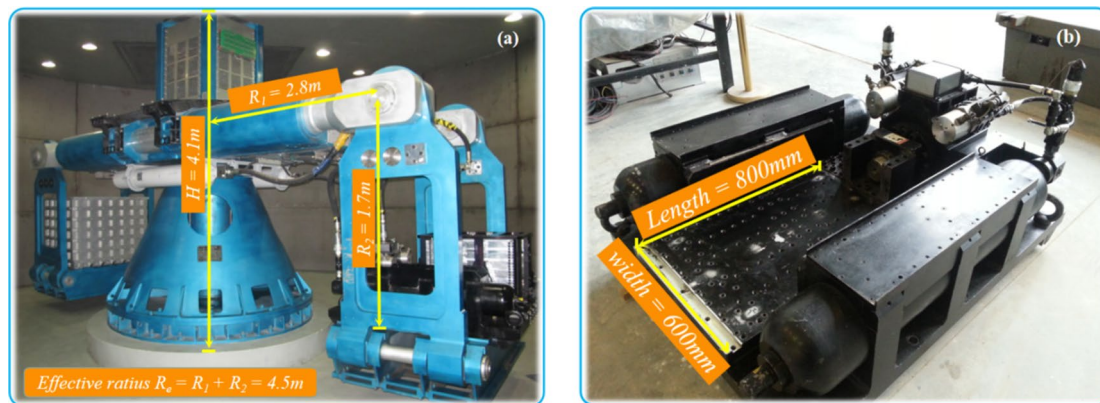
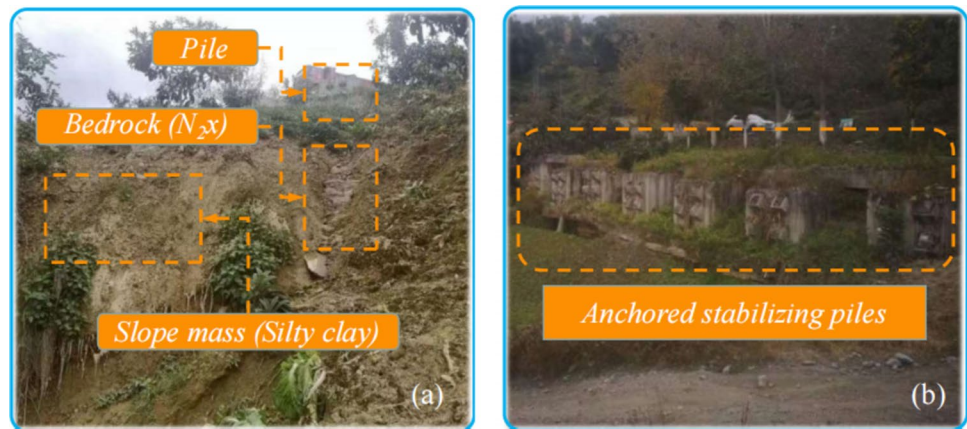


Fig. 3 Test equipment: a centrifuge and b shaking table

material has been proved in other centrifuge tests (Cilingir and Madabhushi 2011). In this research, the thickness of the absorbing material was 25 mm.

Model preparation and materials

The purpose of the model tests is to explore the seismic response characteristics of the anchor-pile-slope system based on a real nonhomogeneous slope. Therefore, most of

the design characteristics of the slope model, such as the material of the slope mass, the design parameters of the pile, and the geometry of the bedrock surface, are consistent with those of the prototype according to the scaling laws (as shown in Table 1). The typical profile of the test model is presented in Fig. 4.

The model consisted of four parts: slope mass, bedrock, piles, and anchor cables. The total height of the test model was 390 mm, while the slope height was 270 mm. The front and back edges of the slope were respectively 115 mm and 195 mm in length, with a slope angle of about 25°. The bedrock lay below the slope mass with a three-part polyline and the dip angles were respectively 54°, 35°, and 11° from top to bottom.

The clayey soil for the slope body is collected from the landslide site and the soil is remodeled according to the same density and moisture content as the prototype. In the model tests, the bedrock was difficult to simulate using the prototype material, so a mixture of clay, cement, quartz sand, and water is used to represent the underlying bedrock, with the optimal weight mixing ratio of 1: 0.55: 1: 0.25, according to several mixing tests. The geotechnical parameters of the slope body and bedrock are measured by laboratory tests, as shown in Table 2. Noted that the measured parameters of the prototype bedrock vary significantly due to the different weathering degrees, so the average value is used. As can be seen, the modulus and shear strength parameters of the

Table 1 Scaling laws for the centrifuge tests

Physical quantity	Symbol	Similarity scale (model/prototype)
Length	L	1/50
Area	A	1/50 ²
Volume	V	1/50 ³
Displacement	u	1/50
Axial force	F	1/50 ²
Bending moment	M	1/50 ³
Section moment of inertia	I	1/50 ⁴
Stress	σ	1
Strain	ϵ	1
Time (dynamic)	t	1/50
PGA	A_{max}	50
Frequency	F_{req}	50

Fig. 4 Geometry of the reinforced slope

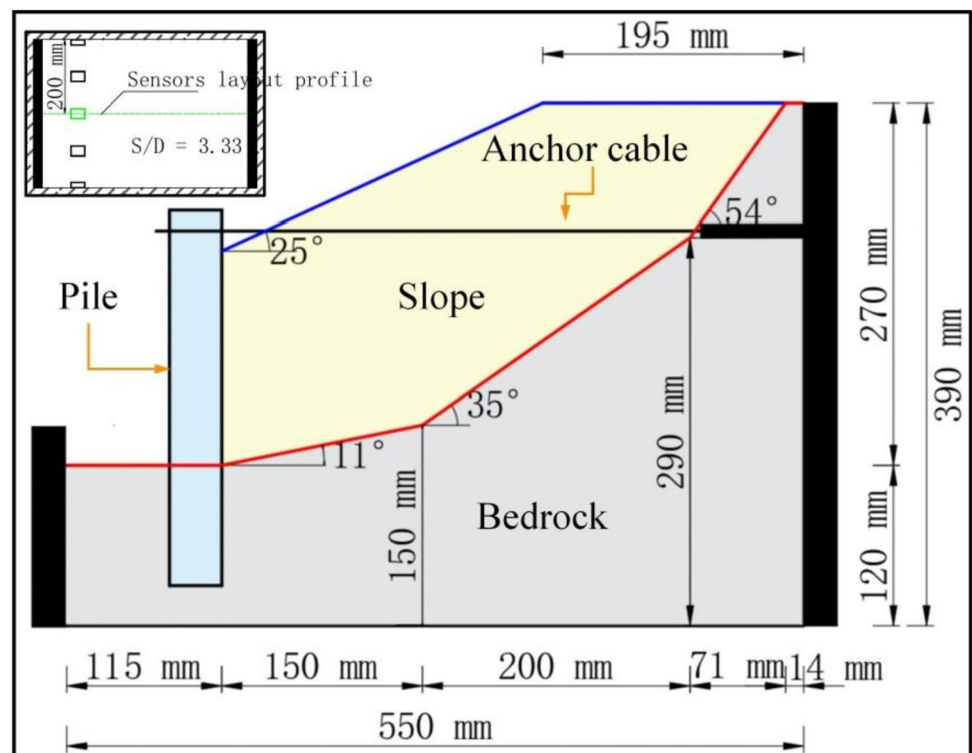


Table 2 Properties of the slide mass and bedrock

Property	Slope mass	Bedrock (prototype)	Bedrock (model)	Slope-bedrock interface (model)
Unit weight γ (kN/m ³)	17.9	18.6	18.6	
Cohesion c (kPa)	48	244	257	3.58
Internal friction angle φ (°)	22	34.7	40.5	14.7
Young's modulus E (Pa)	17.26×10^6	761×10^6	836×10^6	
Poisson ratio ν	0.3	0.27	0.25	
Uniaxial compression strength (MPa)	-	6.3	11.7	

model bedrock are slightly higher than the average value of the prototype bedrock.

In this study, the seismic response characteristic of the pile is the main research purpose, the crack, and fracture of the pile are not considered, thus the aluminum alloy hollow tube with a rectangular cross-section is utilized to simulate concrete piles. To ensure that the model pile reflects the true stress level of prototype one, the dimensions and flexural stiffness of the model pile are designed based on the similarity law. Based on the geometric similarity, the height of the rectangular section of the model pile (h_m) is 40 mm, the width (b_m) is 30 mm, and the length of the pile (l_m) is 280 mm. Based on flexural stiffness similarity (Huang and Zhu 2016), the wall thickness of the model pile can be calculated as follows:

$$E_p I_p = N^4 E_m (b_m h_m^3 - (b_m - 2t_m)(h_m - 2t_m)^3 / 12) \quad (1)$$

where E_p and I_p are Young's modulus and inertia moment of the prototype pile, E_m is Young's modulus of the model pile (i.e., 69 GPa). Based on Eq. 1, the wall thickness of the model pile (t_m) is approximately 2.5 mm. Before the model construction, a specially designed device was used to fix the model pile at the designated location of the model box, and the fixed device was removed after the model was established. Five model piles were used in the test corresponding to the ratio of space to width (i.e., S/D) equals 3.33. The embedded and cantilever section of the pile was 90 mm and 190 mm, respectively. It should be noted that the design parameters of the prototype anchor cable are unknown, so the design of the

model anchor cable refers to existing model tests (Qu et al. 2018; Huang et al. 2020b). The free and anchored sections of the anchor cable are modeled with steel strands (1-mm diameter) and solid steel columns (4-mm diameter), respectively. The steel strand was arranged horizontally: one end was connected to a bolt that was installed at the pile head and another end of the strand was embedded in the bedrock and linked with the anchorage. To avoid the pullout of the anchor cable during shaking, four barbs were manufactured at the fixed end to increase anchorage force. To avoid the generation of friction forces between the soil and the steel strand, the free section of the anchor was covered with a plexiglass casing (diameter of 3 mm). The detailed parameters of the model pile and anchor cable are presented in Table 3.

Measuring devices

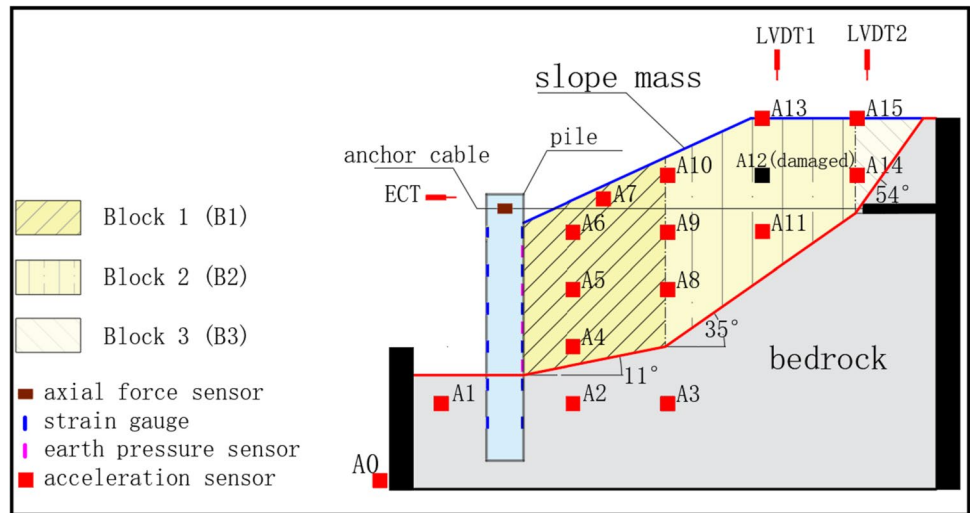
Different kinds of measuring devices were used to collect the response data of the pile-anchor-slope system during earthquake loading, including micro-acceleration sensors, micro-earth pressure sensors, strain gauges, and LVDTs (linear variable differential transformers). Figure 5 shows the typical layout with the locations of sensors.

The model slope was instrumented with 16 horizontal accelerometers, located in the slide mass and the bedrock. The accelerometer A0 was tightly connected to the shaking table, to measure the actual input motion at the rigid basement. To capture the pile bending moment, six pairs of strain gauges (Y1 ~ Y6) were pasted symmetrically on the

Table 3 Parameters of the model pile and anchor cable

Structural elements	Material	Geometric parameters (model/prototype)	Mechanical parameters (model/prototype)
Pile	Aluminum alloy tube	Cantilever length: 190 mm/9.5 m	$EI = 4.9 \times 10^{-3} \text{ MN}\cdot\text{m}^2 / 3.0 \times 10^4 \text{ MN}\cdot\text{m}^2$
Anchor cable	Steel strand	Embedded length: 90 mm/4.5 m Section size: 30 mm × 40 mm/1.5 m × 2 m Thickness: 2.5 mm/- Anchored section: 80 mm/4 m Free section: 354 mm/17.7 m Diameter: 1 mm/5 cm	Tensile strength = 648 MPa/648 MPa Tension force = 49N/122.5kN

Fig. 5 Layout of the reinforced slope



front and back surfaces of the pile with a vertical spacing of 40 mm. Note that all the strain gauges were connected by a full-bridge type. Four T-type micro-earth pressure sensors (T1-T4) were inserted into the cantilever section of the pile with a vertical spacing of 40 mm. To reduce the soil arching effect, the earth pressure sensors and the measured pile were placed in the same plane. The detailed layout of the strain gauges and earth pressure sensors is shown in Fig. 6.

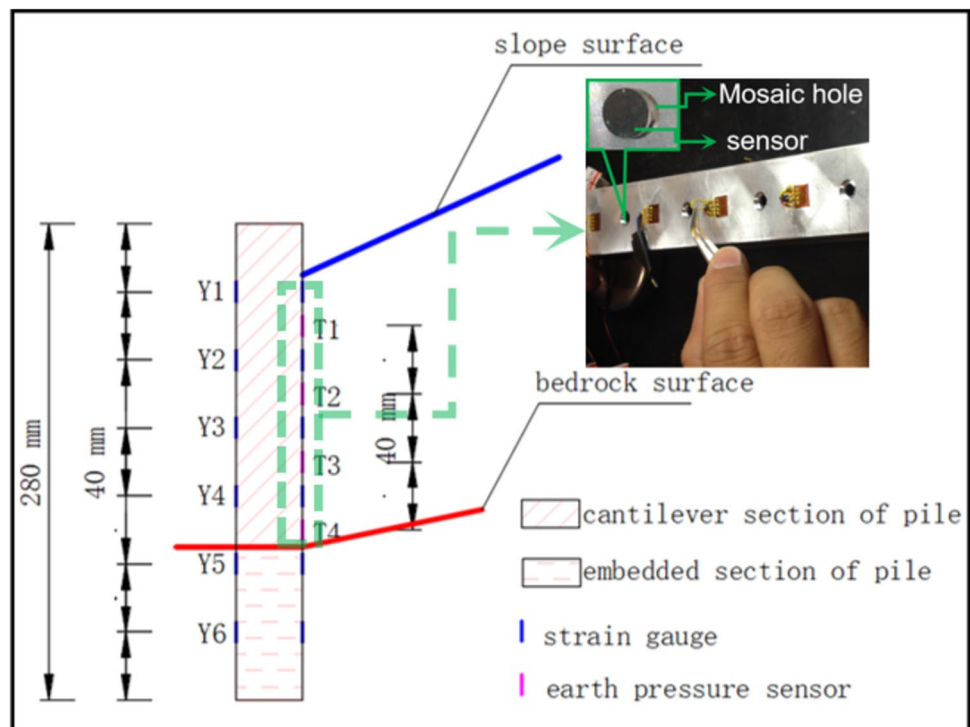
A sheet axial force sensor was used to measure the axial force of the anchor cable. It was made of aviation aluminum alloy and molded by wire-cutting technology. The thickness of the sensor was 1 mm, and the measuring element was a

pair of strain gauges pasted on opposite sides of the sheet. To monitor the vertical settlement of the soil slope and the horizontal displacement of the pile head, two LVDTs and an ECT (eddy current transducer) were arranged on the slope top and pile head respectively (Fig. 5). Besides, a film system with a fast digital camera and a video was used to record the slope damage process during shaking (Fig. 7).

Model earthquakes

Previous studies generally used sinusoidal waves to investigate the seismic response of slopes. However, recent

Fig. 6 Strain gauges and earth pressure transducers



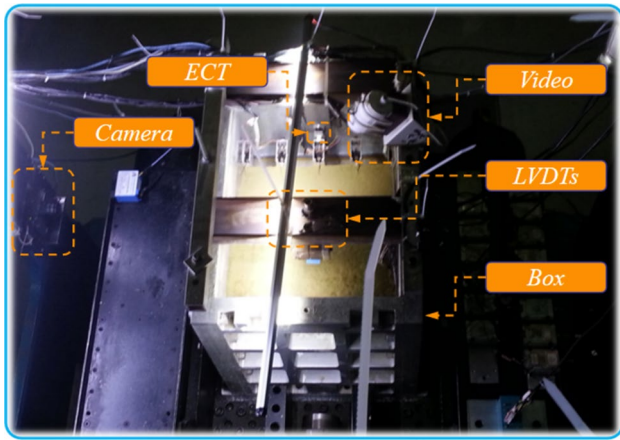


Fig. 7 Model container, fast camera, and model slope

research highlighted that real ground motions, particularly for pulse-like waves and mainshock-aftershock sequences, could aggravate the seismic effect on the slopes (Al-Defae et al. 2013; Bao et al. 2021; Zhu et al. 2020, 2022). Therefore, real ground motion is used in the tests. The input seismic motion was the Qingxi ground motion (about 25 km far from Hanyuan County) in the NS direction, which was recorded in the Wenchuan earthquake. According to the scaling laws for the centrifuge tests, the amplitude and duration of the prototype wave were amplified and shortened respectively by 50 times to convert into the model ground motion. To consider the influence of ground motion intensity on the slope model, the amplitude of the input ground motion was adjusted, ranging from 0.1 to 0.4 g (prototype).

The tests were carried out when the centrifuge acceleration was up to 50 g. As mentioned above, the actual input ground motions were recorded by accelerometer A0. As an example, Fig. 8 shows the measured acceleration time

history and the corresponding Fourier amplitude spectrum for the EQ1 event. Table 4 shows the features of the earthquakes applied to the centrifuge tests, including the amplitude, predominant period, and 90% energy duration of each input ground motion for the prototype. Note that two ground motion scenarios are considered during the centrifuge model tests. The first one is the continuous loading, to study the effect of the motion intensity on the system’s seismic response. The motion intensity gradually increases as the seismic event increases, such as EQ1 ~ EQ3 and EQ4 ~ EQ5, with amplitudes increasing by 0.1 g. The second one is cumulative loading, to consider the cumulative effect of repeated ground motions (Al-Defae et al. 2013; Liang et al. 2015). The motion intensity for adjacent seismic events is the same, such as EQ3 ~ EQ4 and EQ5 ~ EQ7.

Table 4 Model earthquakes

Case No	Amplitude (g)	Predominant period (s)	Duration(s)	Loading condition
EQ1	0.1	0.66	57.92	Continuous loading
EQ2	0.2	0.66	57.92	Continuous loading
EQ3	0.3	0.66	57.92	Continuous loading
EQ4	0.3	0.66	57.92	Cumulative loading
EQ5	0.4	0.66	57.92	Continuous loading
EQ6	0.4	0.66	57.92	Cumulative loading
EQ7	0.4	0.66	57.92	Cumulative loading

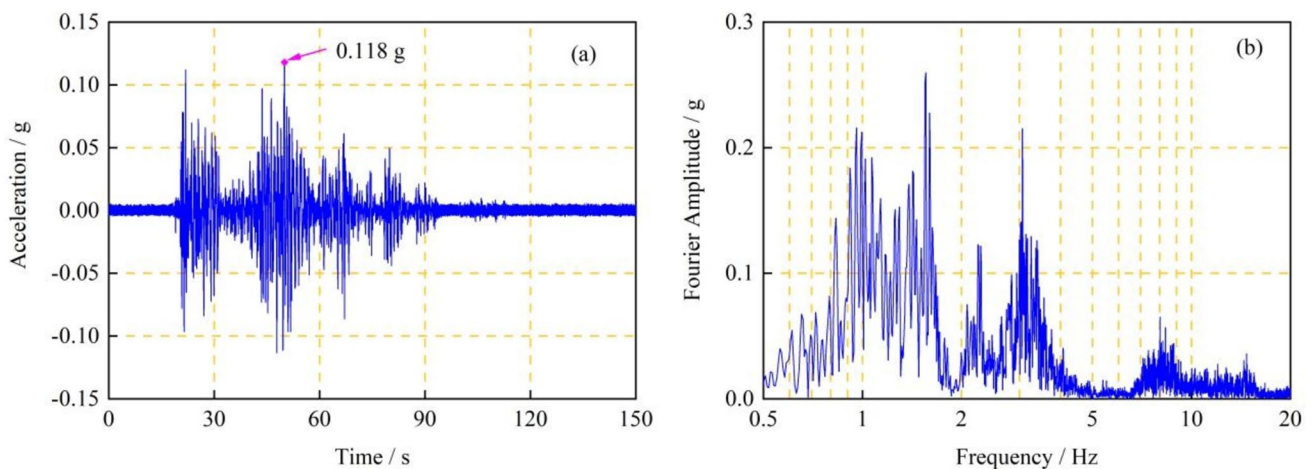


Fig. 8 Measured acceleration time history and the Fourier amplitude spectrum (EQ1)

Results

Model deformations

The vertical settlements of the slope top (LVDT2) and shoulder (LVDT1) and the horizontal displacement of the pile head (ECT) were recorded during earthquake loadings. The evaluations of the deformation of each measuring point corresponding to ground motion sequences EQ1-EQ7 are shown in Fig. 9a. In Fig. 9b, the peak and cumulative deformations of slope shoulder and slope top are shown while Fig. 9c presents the peak and cumulative deformations of the pile head.

Concerning the vertical deformation of the slope, the measured settlement gradually accumulates during the shaking events, with a maximum deformation of 50 mm (prototype scale). Before EQ5, the slope shoulder shows a slightly large deformation than the slope top, as expected. However, the slope shoulder deforms less than the slope top for the cases of EQs 5~7, which can be partly explained by the occurrence and development of cracks. As shown in Fig. 10, a minor crack appears in

the early stage of the shaking while with the increase of ground motion intensity, the number of cracks that have obvious width and depth increases on the slope top surface and inside slope mass. It should be emphasized that the difference in deformation between the slope shoulder and slope top is minor since the reinforced model slope remains stable in this study, and large deformation and instability phenomena are not observed during shaking. In addition, the comparisons of slope deformations for EQ3 with EQ4 and of EQ5 with EQ6 and EQ7 underline the significant influence of loading types (i.e., continuous loading vs cumulative loading) on the slope response. Even if the intensity of input ground motion is the same, cumulative loading appears to result in a decreased settlement in comparison with continuous loading. For instance, the maximum settlement of EQ6 and EQ7 is respectively around 88% and 68% of the value of EQ5, although these three ground motions have the same intensity.

With regard to the horizontal deformation of the pile head, the measured time histories are similar to the input ground motions. With an increasing amplitude of input ground motions, violent vibration of the pile head

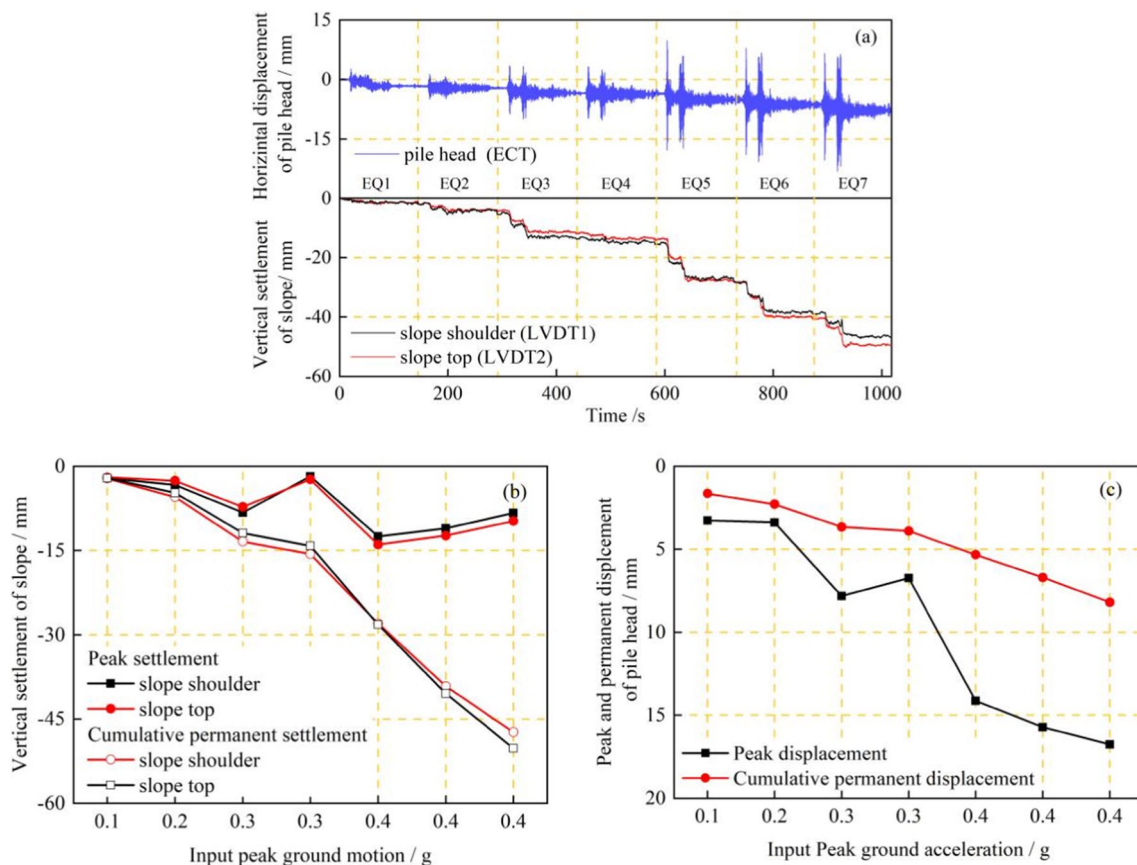
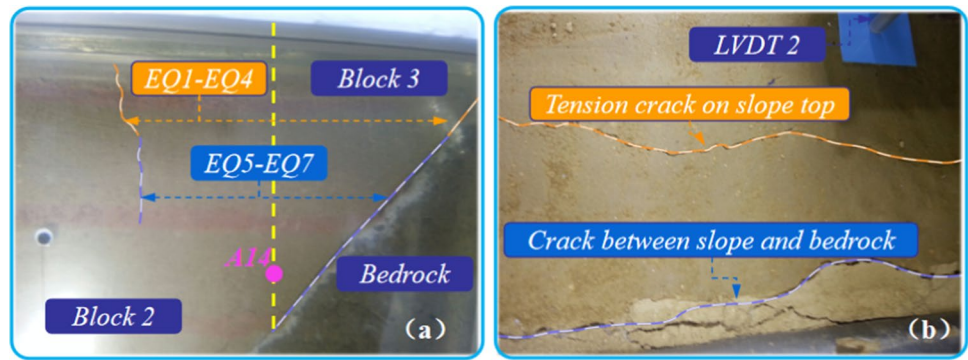


Fig. 9 Responses of the slope and pile head: **a** time histories of the horizontal displacements of pile head and vertical settlements of the slope; **b** peak and cumulative permanent settlements of the slope; **c** peak and cumulative permanent displacements of the pile head

Fig. 10 Development of the cracks during earthquake loadings: **a** side view and **b** top view



(swaying from side to side) occurs during the shaking events with two distinct peaks of deformation. The pile head gradually deforms to the left with the maximum cumulative permanent deformation of up to 8 mm (prototype scale). The deformation accumulation of the pile head is caused by the gradual settlement of the slope mass that is transmitted to the pile (kinematic effect), as indicated in Fig. 9a. Contrary to the peak deformation of the slope, cumulative loading constantly increases the peak deformation of the pile head in comparison with continuous loading for high motion intensity (i.e., 0.4 g). For example, the peak deformation of EQ6 and EQ7 respectively increases from 14 mm of EQ5 to 16 mm and 17 mm.

Accelerations

Acceleration records from the centrifuge tests show that the amplitude of accelerations in the reinforced model slope changes with the positions. To capture the distribution characteristic of acceleration in the reinforced model slope, these changes are evaluated utilizing the contour maps of *PGA* for seven EQ cases. Furthermore, recorded acceleration signals can be used to calculate the cumulative energy of the acceleration at different positions. Arias intensity (I_a) is a physical quantity representing earthquake energy that is commonly utilized in previous studies to measure the total intensity in the recorded ground motions (Arias 1970), which is defined as follows:

$$I_a = \frac{\pi}{2g} \int_0^t a^2(t) dt \tag{2}$$

where g is the acceleration of gravity (m/s^2) and t is the duration (s). To compare the amplification effect of the acceleration response, both the values of *PGA* and I_a are then normalized by the values of a reference position. The normalized amplification factor, α , is calculated using the following formula:

$$\alpha_{x_i} = \frac{\beta_{x_i}}{\beta_{x_0}} \tag{3}$$

where β_{x_i} is the measured value of the ground motion parameter at a certain measuring point x_i and β_{x_0} is the measured ground motion parameter value recorded by sensor A0.

Contour maps of α_{PGA} and α_{I_a} in the slope mass for seven EQ events are presented in Figs. 11 and 12, as the measured values are marked by pink points and then be interpolated to get a distribution map.

It can be seen that the amplification distributions of both *PGA* and I_a share similar characteristics. As shown in Figs. 11 and 12, the seismic energy is amplified for various degrees, depending upon locations, motion intensity, and loading types. From the aspect of morphology, the shape of the contours is wavy and extends obliquely from the cantilever section of the pile to the slope top. This form of the contour is much more nonlinear than that from the horizontal distribution of a homogeneous slope (Brennan and Madabhushi 2009). For each vertical array, the ground motion is amplified when it propagates from the bedrock to the slope surface. The amplification effect is more evident for the first and third vertical arrays due to the combined influence of site effect and topographic effect while the acceleration and cumulative energy are less amplified at the middle of the slope surface (second array) and the slope top (fourth array).

It is possible to see that the maximum amplification factor for *PGA* and I_a is measured at A6 for each EQ case. More specifically, the *PGA* amplification factor increases from 2.11 of EQ1 to 3.25 of EQ7 while the I_a amplification factor increases from 5.11 to 9.1. It appears that the amplification effect is aggravated by increased motion intensity. The focusing of seismic energy within convex topographies (corner of the slope) certainly plays a significant role in the observed amplification effects. On the other hand, the soil-pile kinematic interaction may also contribute to such a high amplification factor. As shown in Fig. 9, the pile deforms

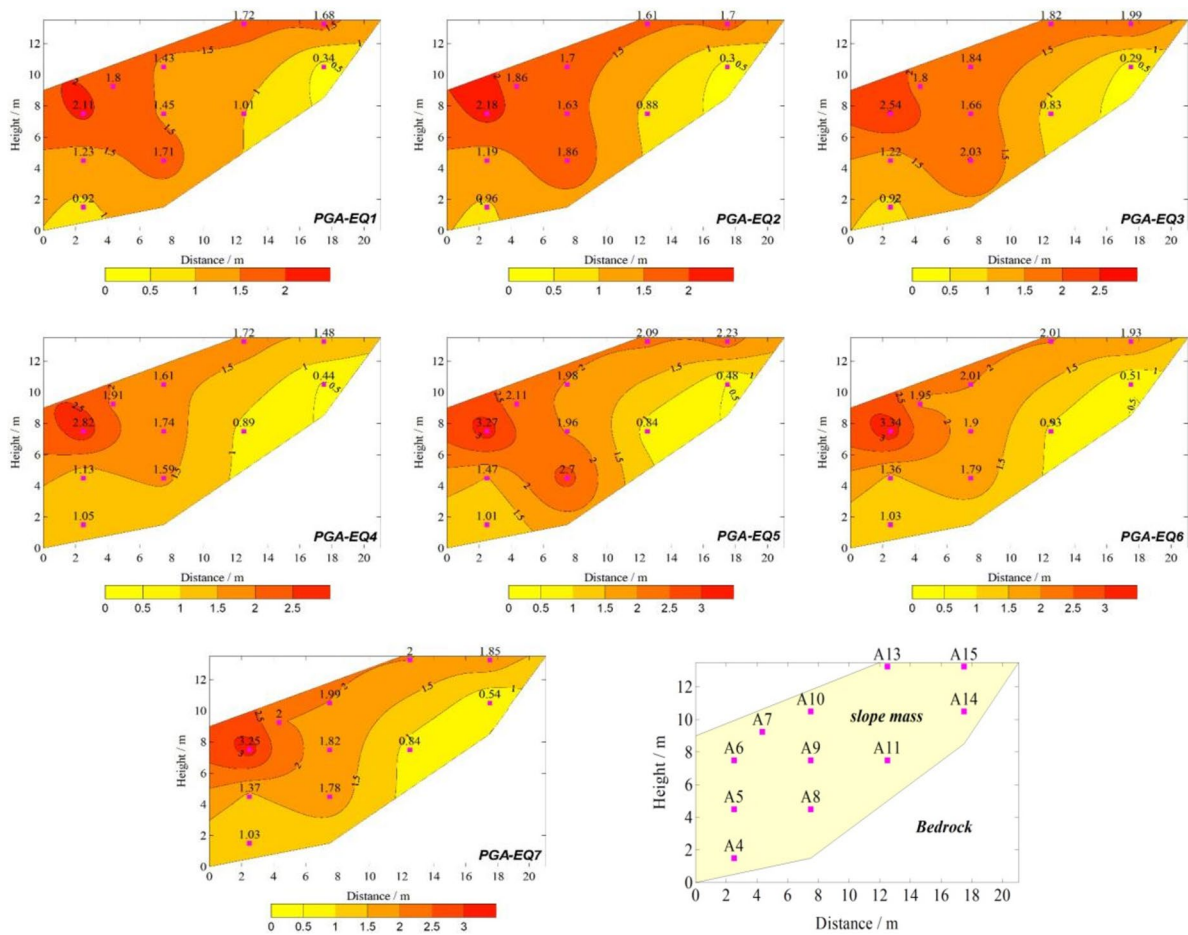


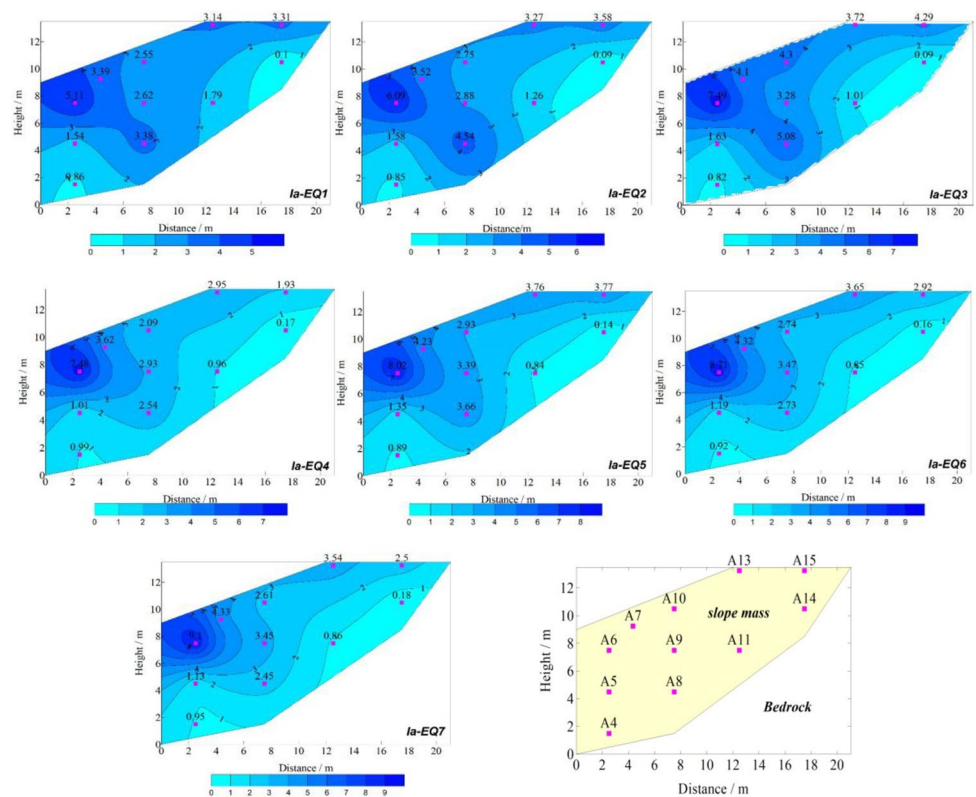
Fig. 11 Contour maps of the *PGA* amplification factors

significantly during the shaking events, which appears to amplify the ground motion nearby. The amplification of ground motion caused by the kinematic effect was also observed in the centrifuge test performed by Cilingir and Madabhushi (2011) in evaluating the soil-tunnel seismic interaction. For the measured points close to the bedrock, the ground motions are always de-amplified. This is generally more evident at point A14, with the amplification ratios of *PGA* changing from 0.29 to around 0.54 while the I_a amplification ratios vary from 0.09 to 0.18. This is understandable because the soil deposit with a thin thickness amplifies less the incoming waves. The inclined bedrock surface (steep dip angle 53°) also significantly reflects the seismic wave and restrains the shaking amplitude of the soil particle thus leading to a small amplitude in the horizontal direction.

To figure out in which frequency range the ground motion is amplified or de-amplified, the spectral ratios are presented for two typical locations in which the maximum or the minimum amplification effect is respectively observed. Figure 13 thus presents the A6 to A0, A14 to A0 spectral

ratios, together with the corresponding Fourier spectra of A0, A6, and A14. These results show very clearly that these spectral ratios are less sensitive to the motion intensity than the location. In the main frequency ranges (around 1.7 Hz, 3.0 Hz), the amplitudes of spectral ratio at A6 range between 2 and 3, while A14 spectral ratios range between 0.2 and 0.5 only. The higher frequency narrowband amplification peaks observed at around 6 Hz are not due to the large amplitude of the Fourier spectrum but to the very small amplitude of A0 around this frequency point. The resonance effect associated with the model slope leads to narrowband amplification of about 12 times for A6 and 2 times for A14 for the case of EQ1. Concerning the influence of motion intensity, a larger spectral ratio is calculated for higher motion intensity, but the frequency corresponding to the peak is almost the same for EQ1 and EQ7 cases. This explains why the ground motion amplification is a little bit large for high motion intensity. In addition, the very similar shapes of the spectral ratios for two motion intensities implicitly indicate that the slope suffers ignorable stiffness degradation during shaking.

Fig. 12 Contour maps of the I_a amplification factors



Static and dynamic earth pressures

Before the shaking events, the earth pressures acting on the pile are measured when the centrifugal acceleration increases from 0 to 50 g. As shown in Fig. 14, the maximum static earth pressure is measured at T1 (158.64 kPa) while the minimum one appears at T4 (39.41 kPa). In current design practice, a uniform distribution of earth pressure (blue dash line in Fig. 14) is generally assumed for a pile-reinforced cohesion soil slope. However, this assumption may be inappropriate according to the centrifuge data performed in the present study. For the test model, the resultant force of 628 kN can be calculated according to the area of the distribution.

An empirical equation is recommended in the design code GB/T 38509–2020 (2020) to estimate the resultant force of the theoretical landslide thrust, which is related to the inclination of the bedrock surface, the strength parameters of the soil-rock surface, and the self-weight of the slope mass, as follows:

$$E_i = E_{i-1}\psi_i + T_i - R_i/F_s \tag{4}$$

$$\psi_i = \cos(\alpha_{i-1} - \alpha_i) - \sin(\alpha_{i-1} - \alpha_i)\tan\phi'_i/F_s \tag{5}$$

$$T_i = W_i \sin\alpha_i \tag{6}$$

$$R_i = W_i \cos\alpha_i \tan\phi' + c_i b_i \sec\alpha_i \tag{7}$$

where E_i is the residual sliding force of the soil strip i (Fig. 15); ψ_i is the transfer coefficient of the sliding thrust between soil strips; α_i is the inclination of soil strip i ; T_i and R_i is the sliding force and anti-sliding force of soil strip i , respectively; W_i is the gravity of soil strip i ; c' and ϕ' is the cohesive and internal friction angle at the slope-bedrock interface (Table 3); and F_s is the safety factor; a value of 1.2 is adopted here according to the design report of the Beihoushan slope reinforcement engineering.

Accordingly, the theoretical resultant force is 534 kN. The differences between the measured thrust and the theoretical one should be attributed to the anchor cable action and soil arching effect. The landslide thrust formed by the self-weight of the slope acts on the pile, resulting in the outward deformation of the pile. The tension of the anchor cable makes the pile-soil squeeze each other, affecting the distribution of earth pressure. In addition, the soil between the model piles is not reinforced by any baffles, which leads to the redistribution of earth pressure (so-called arching effect), and thus affects the pile behavior. The combined effect raised by these factors complicates the distribution form of the pile earth pressure, resulting in the maximum

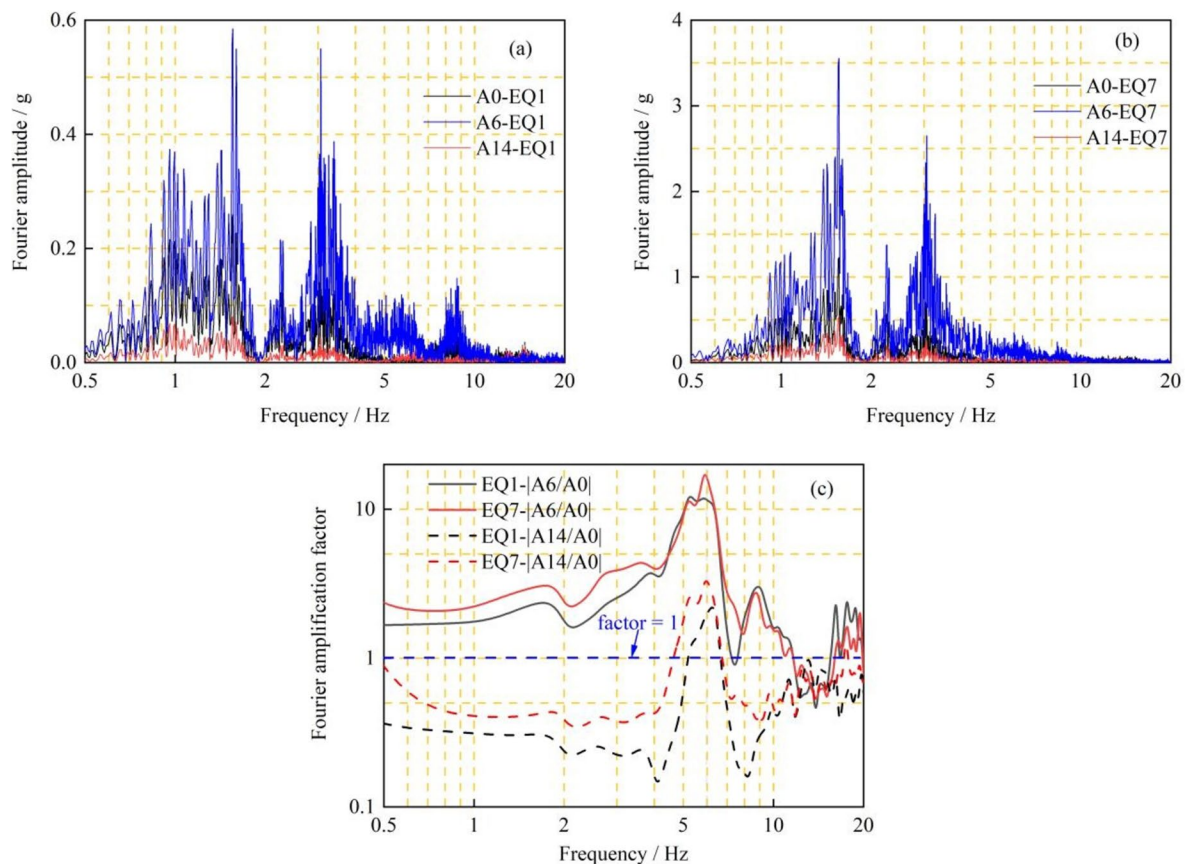


Fig. 13 Fourier spectra of three measured points and the corresponding spectral ratios

passive earth pressure at T1 and the minimum passive earth pressure at T4.

The typical time histories of dynamic earth pressures are presented in Fig. 16, corresponding to the case of EQ7. The dynamic earth pressures are obtained by subtracting the earth pressures measured at the end of the previous event (i.e., EQ6) from those at the end of the current event (i.e., EQ7). It is possible to see that the earth pressures change rapidly for T1 and the earth pressures reach a maximum value at the time of maximum deformation of the pile head. A residual earth pressure is also observed at the end of shaking but the value is relatively small compared to the maximum one. On the other hand, the positive residual earth pressure indicates that the pile prevents the deformation of the slope. The time histories of earth pressure measured at the other three positions show a similar trend, but with decreased amplitudes.

Figure 17 shows the distribution of the maximum dynamic earth pressure (absolute values) on the pile during the earthquake loadings. Maximum dynamic earth pressure is defined as the maximum incremental earth pressure ever

experienced at that specific position during shaking events. It is clear to see that the maximum earth pressure increases with increasing motion intensity. For each event, the distribution of maximum earth pressure follows an inverted trapezoidal distribution. The earth pressure is expected to increase with the increase in height of the model pile, with the maximum earth pressure occurring at the pile head (T1). For example, the measured earth pressures are relatively small and show less variation along with the pile with the maximum earth pressure of around 20 kPa in the case of 0.1 g (EQ1). A dramatic increase in the earth pressure appears with increasing motion intensity, particularly for the pile head at which the maximum earth pressure is up to 180 kPa in the case of 0.4 g (EQ7). The earth pressures on the pile vary significantly, reaching a difference of around 9 times between T1 and T4.

To compare the dynamic earth pressure of the continuous loadings with the cumulative loadings for all the investigated cases, the dimensionless parameter named variation rate of dynamic earth pressure (*VRDEP*) is calculated using the following formula:

Fig. 14 Schematic diagram of pile deformation and earth pressure distribution before shaking

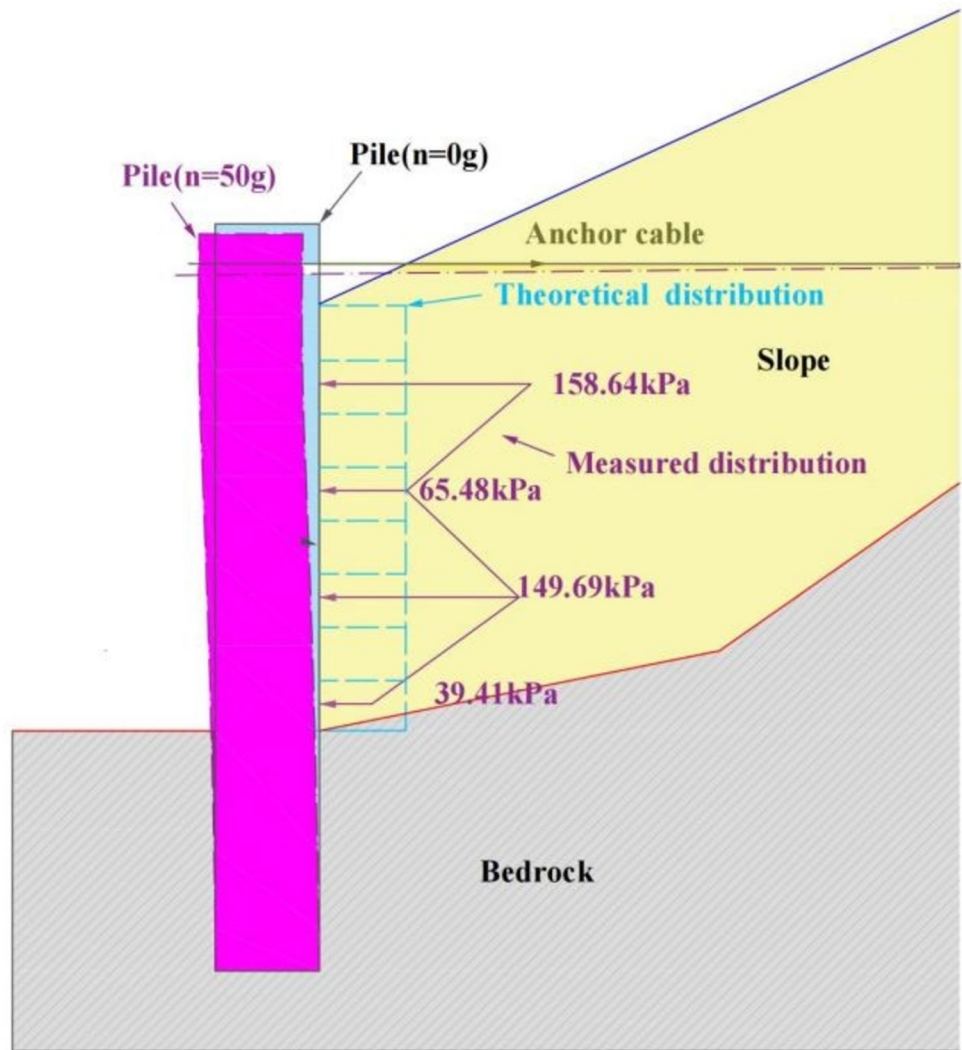
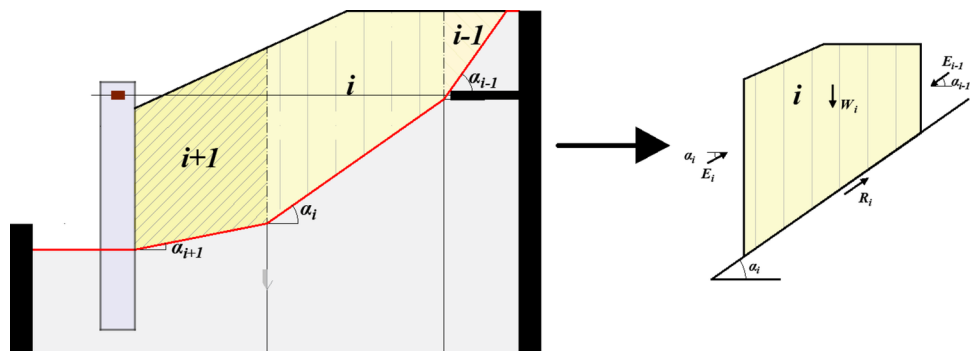


Fig. 15 Schematic diagram of landslide thrust calculation



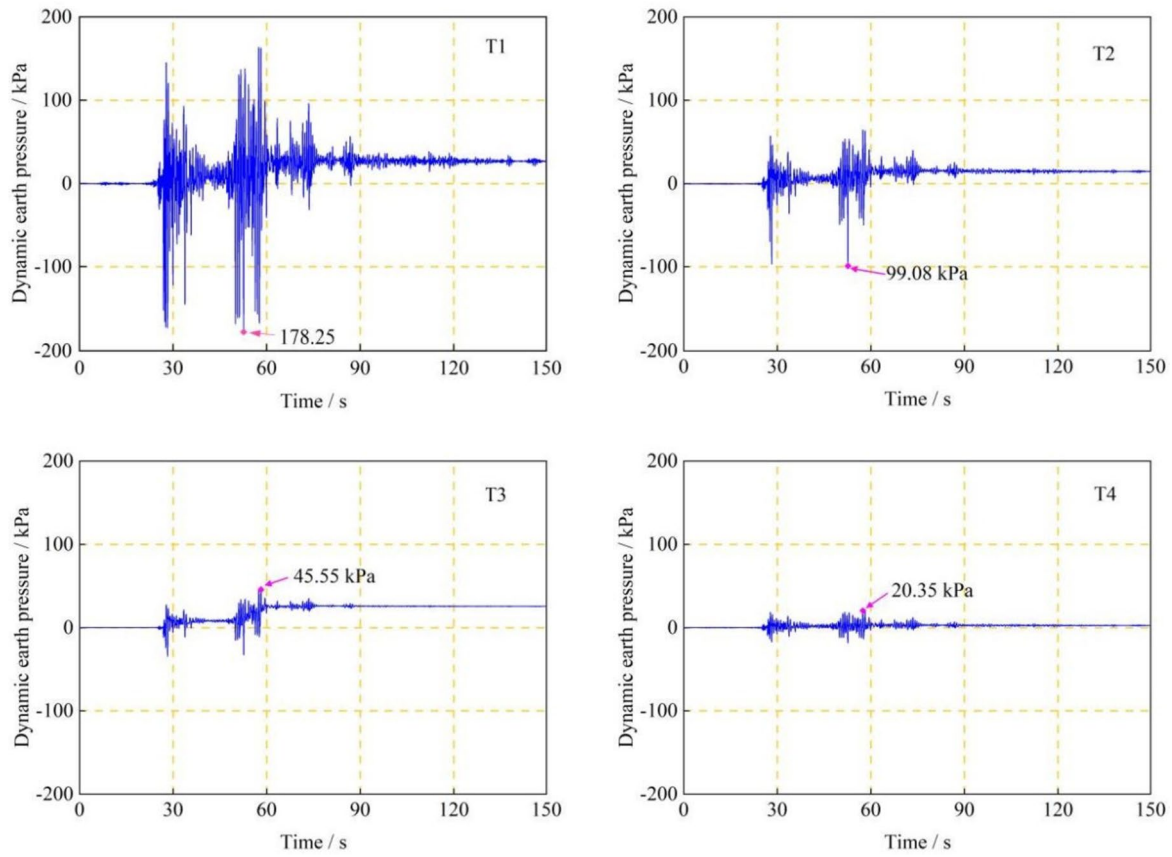


Fig. 16 Time histories of dynamic earth pressure measured in event EQ7

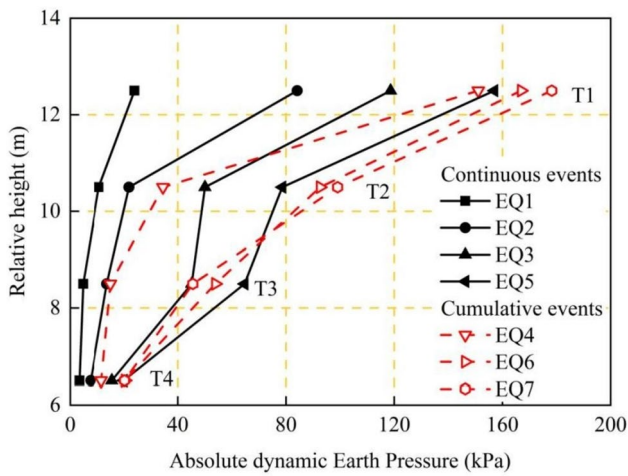


Fig. 17 Absolute maximum dynamic earth pressures on the model pile

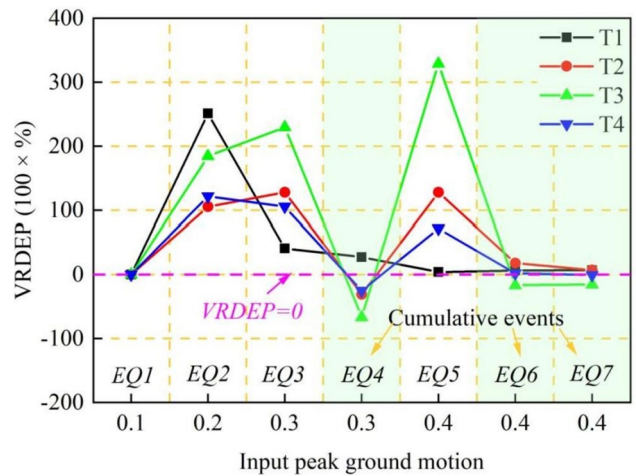


Fig. 18 Calculated VRDEP values for different EQ events

$$VRDEP = \begin{cases} 0 & i = 1 \\ \frac{\gamma_i - \gamma_{i-1}}{\gamma_{i-1}} \times 100\% & i = 2, 3 \dots 7 \end{cases} \quad (8)$$

where γ_i is the maximum earth pressure measured by sensor T_x ($x = 2, 3, 4$) during the earthquake events and the $VRDEP$ is equal to 0 for the EQ1 event.

The results of $VRDEP$ are shown in Fig. 18. It is possible to divide these values into two categories. The first category is the $VRDEP$ of T1 for which the maximum of 250% appears for EQ2, while significantly decreasing with increasing motion intensity. The positive values calculated for EQ4, EQ6, and EQ7 indicate that the cumulative loading results in additional earth pressure due to the cumulative deformation of the slope (Fig. 9b). The remaining values relevant to sensors T2–T4 are the second category for which the motion intensity and loading type significantly affect the values. For continuous loading cases (EQ1 ~ EQ3, EQ4 ~ EQ5), the dynamic earth pressures increase sharply with increasing motion intensity. The influence is more evident for T3, with a maximum value of around 300%. However, for cumulative loading cases (EQ3 ~ EQ4, EQ5 ~ EQ7), the earth pressures are generally reduced to a certain degree. The comparison of earth pressures of T1 with other sensors highlights that the anchor cable has capable of inhibiting the build-up of earth pressure around the pile head. This helps to maintain the integrity of the slope, but can also lead to further dynamic compression between the pile and the soil, resulting in a rapid increase in local earth pressure (e.g., T2 and T3).

Dynamic bending moments

Bending moments acting on the pile are measured at six discrete positions during shaking events. Figure 19 shows the variation of dynamic bending moments for event EQ7. These bending moments are additional incremental values over the previous shaking events as previously mentioned for the dynamic earth pressures. The positive value means the pile deforms toward the slope and vice versa. Similar to the dynamic earth pressure, the time histories of bending moment also capture two peaks during shaking and have small residual bending moments at the end of the shaking event.

Figure 20 shows the distribution of maximum dynamic bending moments in the model pile during EQ1–EQ7. Maximum bending moment is defined as the maximum incremental bending moment ever experienced at that specific position during the current shaking event. Both the negative and positive bending moments are evaluated rather than the absolute one; in this way, the stress state in the model pile can be assessed.

As can be seen, the bending moments are generally positive, except Y1, due to the slope deformation acting on the model pile, as discussed in Fig. 9. The negative bending moment in the pile head (Y1) is caused by the kinematic constraint that comes from the anchor cable. However, due to the high rigidity of the model pile and no obvious slope deformation during shaking, resulting in this bending moment is small. Along with the pile, there is a conversion point with a value of zero between Y1 and Y2, and the positive bending moments gradually increase and reach a maximum value near the interface between bedrock and soil layers. In general, the maximum bending moment is measured by Y4 because of the significant stiffness difference between the soil and bedrock. For the pile part that is fixed in the bedrock, the bending moments (Y5 and Y6) appear to gradually decrease.

The distribution of the dynamic bending moments depends on the pattern of deformation the model pile experiences during the shaking events. The maximum bending moment increases with increasing ground motion intensity, except in the case of EQ4. As shown in Fig. 9c, the peak deformation of the pile head in the EQ4 event is relatively small compared to the one in the EQ3 case. Oppositely, the cumulative loadings lead to a considerable increase in the maximum bending moment for high motion intensity (0.4 g), the maximum bending moment increases from 4.7 MN·m of EQ5 to around 5.4 MN·m of EQ7, with a percent increase of 15%.

Axial forces of anchor cable

The axial force of the anchor cable is measured at the cable’s left head using strain gauges as previously mentioned. Figure 21 presents the peak axial force for each EQ event, together with the time histories of axial force for EQ7. It appears that the peak axial force of the anchor cable increases with increasing motion intensity. This is more evident for the cumulative loading case due to the increased cumulative deformation of the pile head as shown in Fig. 9c. Residual axial force lefts on the anchor cable, indicating the anchor cable is in an extension state to remain stable of the pile at the end of shaking.

Regression analyses are also performed to figure out how the pile head deformation and slope settlement affect the axial force of the anchor cable. The results are shown in Fig. 22. It is possible to see that the axial force of the anchor cable and peak deformation of the pile head have a very strong linear correlation. It shows that the goodness of fit of the first-order linear equation is close to 0.92. The increase of axial forces with increasing slope settlements is generally observed, but they show a large variation with a coefficient of determination less than 0.6. It is understandable since the settlements measured in this study are not mainly caused by

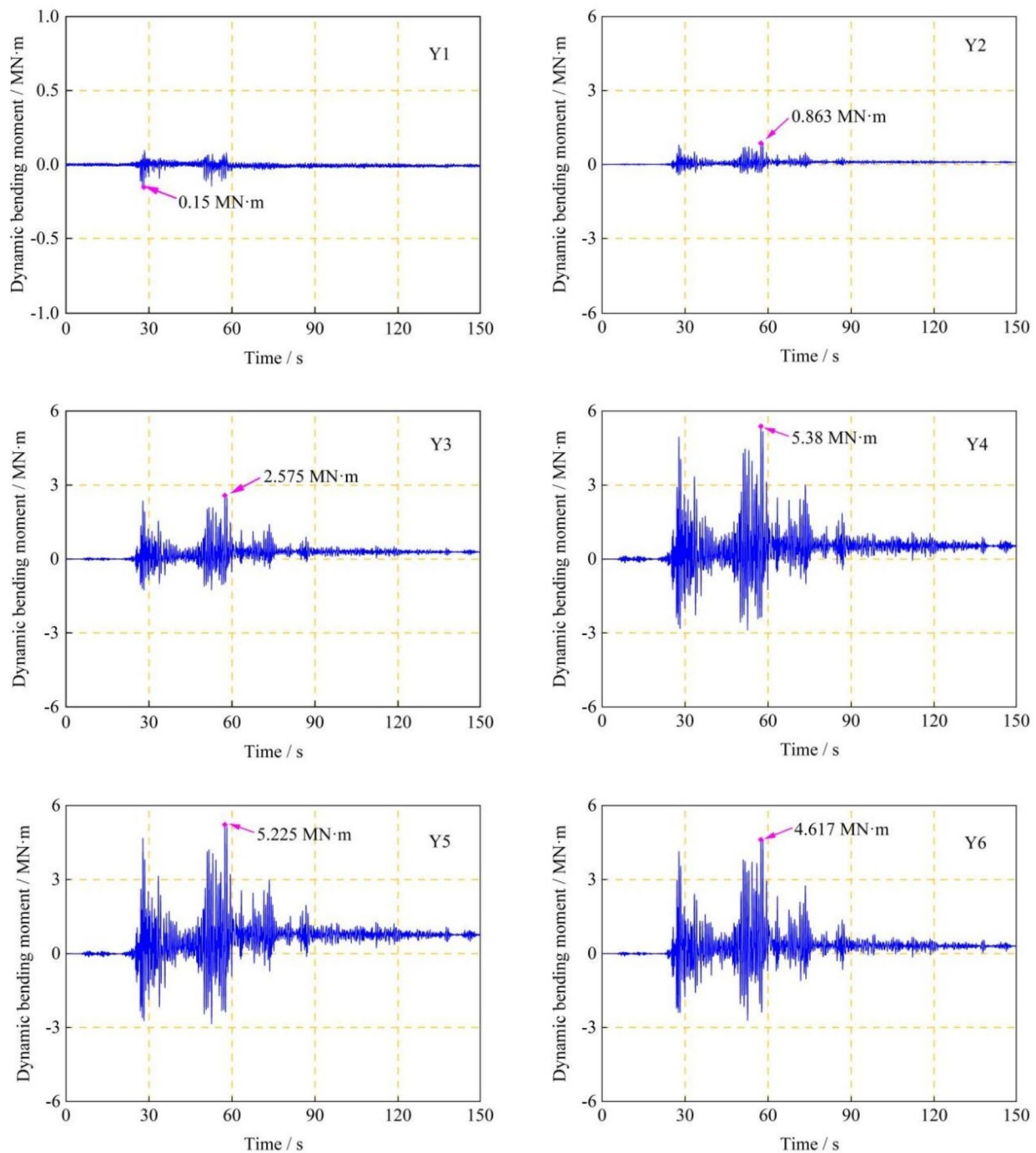


Fig. 19 Time histories of dynamic bending moment on the pile in EQ7

slope instability, the soil densification, and cracks developed during shaking contribute a lot. The results highlight that it is possible to estimate the axial force of anchor cable based on the deformation of the pile head for a specific reinforced slope. It also indicates that the coordinated deformation between pile and anchor cable still exists during earthquake events.

Conclusions

A series of centrifuge shaking table tests were performed to investigate the seismic response of a slope with a polyline bedrock surface reinforced by anchored piles. The response characteristics in terms of deformations of pile and slope, distributions of the PGA and I_a amplification factors, earth

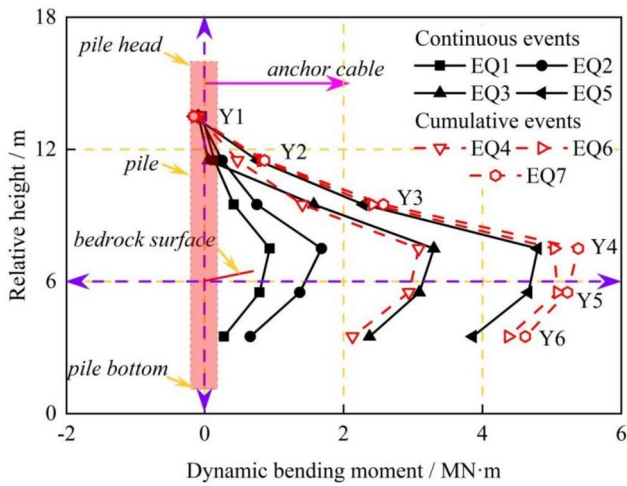


Fig. 20 Maximum dynamic bending moment acting on the pile

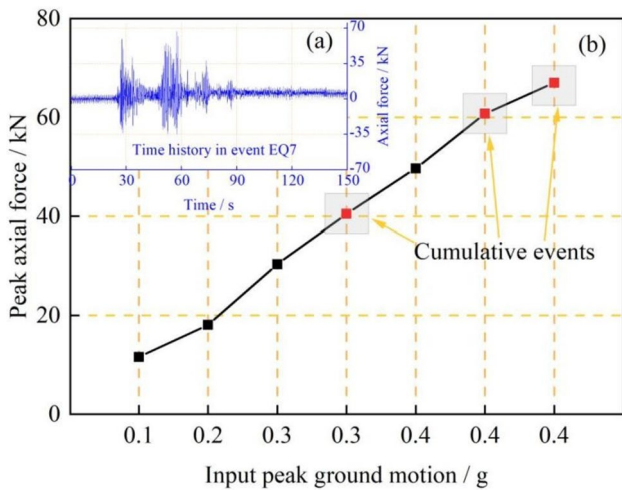


Fig. 21 Axial force–time history of the anchor cable and the relationship between the peak axial force and motion intensity

pressures, bending moments of the pile, and axial forces of anchor cable were measured and analyzed, accounting for different motion intensities and loading types. The main conclusions can be summarized as follows:

1. The vertical settlement of the slope and deformation of the pile head increased gradually with increasing motion intensity due to soil densification and cracks developed during the shaking events. In addition, cumulative loading constantly increased the peak deformation of the pile head for high motion intensity. The increased peak deformation of the pile head was caused by the increased slope settlement.
2. Due to the combined effects of the site and topographic, the amplification factors near the slope surface were more evident, particularly at the position near the pile head. The soil-pile kinematic interaction may also contribute to such a high amplification effect. This led to a wavy-form distribution of acceleration. The spectral ratios for two motion intensities indicated that the slope suffers ignorable stiffness degradation during the shaking events.
3. The distribution of the peak dynamic earth pressure of the cantilever section of the pile was presented as the “inverted trapezoid,” and the maximum one was measured at the pile head. The maximum earth pressure tended to increase with increasing motion intensity. Also, the cumulative loadings resulted in a higher dynamic earth pressure compared to the continuous loadings.
4. The bending moments were significantly affected by the presence of the anchor cable and the soil-rock interface. Near the pile head, negative bending moments were observed due to the restrain caused by the anchor cable, with the bending moments increased with depth, and the maximum value was measured around the soil-rock interface due to the large stiffness difference.
5. The axial force of anchor cable can be well estimated based on the peak deformation of the pile head, rather than the settlement of the slope. Residual axial force observed at the end of the shaking showed that the anchor cable is in an extension state to remain the stability of the pile.

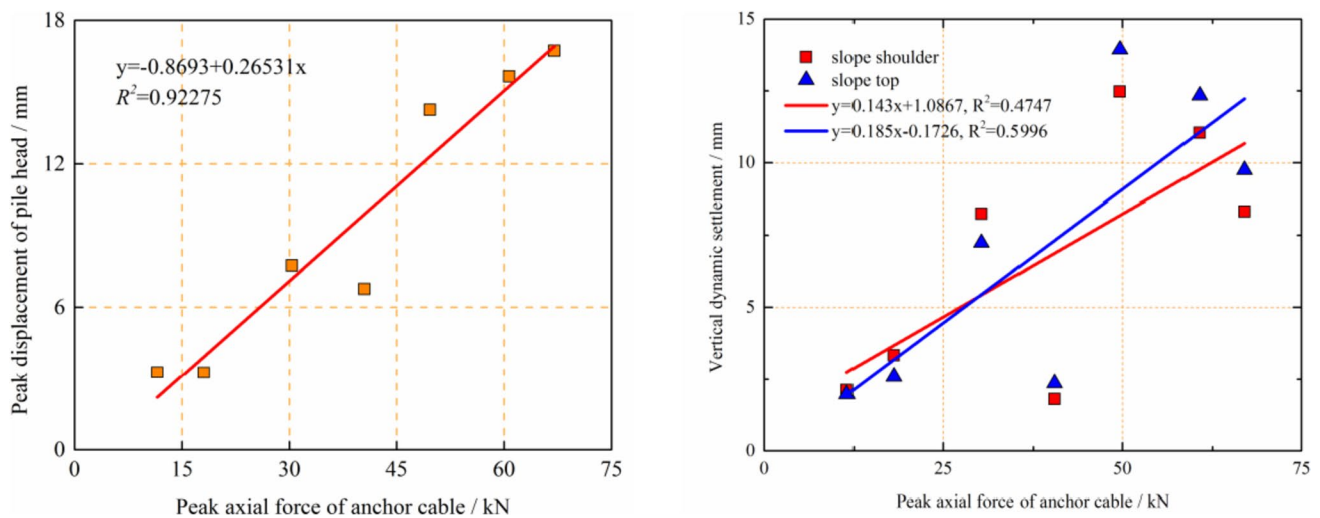


Fig. 22 Relationships between the peak axial force of anchor cable with the peak displacement of pile head and the peak settlements of the slope

Funding This work was supported by the Scientific Research Fund of the Institute of Engineering Mechanics, China Earthquake Administration (Grant No. 2020C02), the National Natural Science Foundation of China (Grant No. 51808515 and 41172293), the Joint Guiding Project of Natural Science Foundation of Heilongjiang Province (Grant No. LH2020E020), the Natural Science Foundation of Hebei Province (Grant No. E2020201017), and Hebei Provincial University Science and Technology Research Project (Grant No. ZD2020157).

Data Availability The data that support the findings of this study are available on request from the corresponding author.

References

- Al-Defae AH, Caucis K, Knappett JA (2013) Aftershocks and the whole-life seismic performance of granular slopes. *Geotechnique* 63(14):1230–1244
- Arias A (1970) A measure of earthquake intensity. In: Hansen RJ (ed) *Seismic design for nuclear power plants*. MIT Press, Cambridge, pp 438–483
- Bao YJ, Huang Y, Zhu CQ (2021) Effects of near-fault ground motions on dynamic response of slopes based on shaking table model tests. *Soil Dyn Earthq Eng* 149:106869
- Bi J, Luo XQ, Zhang HT, Shen H (2019) Stability analysis of complex rock slopes reinforced with prestressed anchor cables and anti-shear cavities. *Bull Eng Geol Env* 78:2027–2039
- Brennan AJ, Madabhushi SPG (2009) Amplification of seismic accelerations at slope crests. *Can Geotech J* 46:585–594
- Cilingir U, Madabhushi SPG (2011) Effect of depth on seismic response of circular tunnels. *Can Geotech J* 48:117–127
- GB/T 38509-2020 (2020) Code for the design of landslide stabilization. Industry Standard Compilation Group of the People's Republic of China, Beijing
- Huang RQ, Li WL (2009) Analysis of the geo-hazards triggered by the 12 May 2008 Wenchuan Earthquake, China. *Bull Eng Geol Env* 68(3):363–371
- Huang Y, Xu X, Mao W (2020a) Numerical performance assessment of slope reinforcement using a pile-anchor structure under seismic loading. *Soil Dyn Earthq Eng* 129:1–7
- Huang Y, Xu X, Liu J, Mao W (2020b) Centrifuge modeling of seismic response and failure mode of a slope reinforced by a pile-anchor structure. *Soil Dyn Earthq Eng* 131:1–11
- Huang Y, Zhu CQ (2016) Safety assessment of antiliquefaction performance of a constructed reservoir embankment. I: experimental assessment. *J Performance Construct Facilities* 31(2):04016101
- Huang MH, Fielding EJ, Liang CR, Milillo P, Salzer J (2017) Coseismic deformation and triggered landslides of the 2016 Mw 6.2 Amatrice earthquake in Italy. *Geophys Res Lett* 44(3):1266–1274
- Kang GC, Song YS, Kim TH (2009) Behavior and stability of a large-scale cut slope considering reinforcement stages. *Landslides* 6(3):263–272
- Kawashima K, Aydan Ö, Aoki T et al (2010) Reconnaissance investigation on the damage of the 2009 L'Aquila, central Italy earthquake. *J Earthquake Eng* 14(6):817–841
- Keefer DK (1984) Landslides caused by earthquakes. *Geol Soc Am Bull* 95(4):406–421
- Keefer DK (1994) The importance of earthquake-induced landslides to long-term slope erosion and slope-failure hazards in seismically active regions. *Geomorphology* 10(1):265–284
- Liang T, Knappett JA, Duckett N (2015) Modelling the seismic performance of rooted slopes from individual root-soil interaction to global slope behaviour. *Geotechnique* 65(12):995–1009
- Liu HS, Bo JS, Li P, Qi WH, Zhang YD (2016) Site amplification effects as an explanation for the intensity anomaly in the Hanyuan Town during the Wenchuan Mw 7.9 earthquake. *Earthquake Engng Vib* 15(3): 435–444
- Pai LF, Wu HG (2021) Shaking table test of comparison and optimization of seismic performance of slope reinforcement with multi-anchor piles. *Soil Dynam Earthquake Eng*:106737
- Qu HL, Luo H, Hu HG, Jia HY, Zhang DY (2018) Dynamic response of anchored sheet pile wall under ground motion: analytical model with experimental validation. *Soil Dyn Earthq Eng* 115:896–906
- Sharma K, Deng L (2019) Reconnaissance report on geotechnical engineering aspect of the 2015 Gorkha, Nepal, earthquake. *J Earthquake Eng* 23(3):512–537
- Shrestha S, Kang TS (2019) Assessment of seismically-induced landslide susceptibility after the 2015 Gorkha earthquake. *Nepal Bull Eng Geol Environ* 78:1829–1842
- Siller TJ, Christiano PP, Bielak J (1991) Seismic response of tie-back retaining walls. *Earthquake Engng Struct Dynam* 20(7):605–620

- Song YS, Hong WP, Woo KS (2012) Behavior and analysis of stabilizing piles installed in a cut slope during heavy rainfall. *Eng Geol* 129–130:56–67
- Tang C, Zhu J, Qi X, Ding J (2011) Landslides induced by the Wenchuan earthquake and the subsequent strong rainfall event: a case study in the Beichuan area of China. *Eng Geol* 122(1–2):22–33
- Tsai CC, Hsu SY, Wang KL, Yang HC, Chang WK, Chen CH, Hwang YW (2018) Geotechnical Reconnaissance of the 2016 M_L 6.6 Meinong Earthquake in Taiwan. *J Earthquake Eng* 22:9:1710–1736
- Usluogullari OF, Temugan A, Duman ES (2016) Comparison of slope stabilization methods by three-dimensional finite element analysis. *Nat Hazards* 81(2):1027–1050
- Wartman J, Dunham L, Tiwari B, Pradel D (2013) Landslides in Eastern Honshu Induced by the 2011 Tohoku Earthquake. *Bull Seismol Soc Am* 103(2B):1503–1521
- Yang Z, Liu G, Wang LY, Liu SH, Fu XL (2021) Evolution of hydro-mechanical behaviours and its influence on slope stability for a post-earthquake landslide: implications for prolonged landslide activity. *Bull Eng Geol Env* 80:8803–8822
- Ye S, Fang G, Zhu Y (2019) Model establishment and response analysis of slope reinforced by frame with prestressed anchors under seismic considering the prestress. *Soil Dyn Earthq Eng* 122:228–234
- Yin YP, Wang FW, Sun P (2009) Landslide hazards triggered by the 2008 Wenchuan earthquake, Sichuan. *China Landslides* 6(2):139–152
- Yin YP, Li B, Wang WP (2015) Dynamic analysis of the stabilized Wangjiayan landslide in the Wenchuan Ms 8.0 earthquake and aftershocks. *Landslides* 12(3):537–547
- Zhang CL, Jiang GL, Su LJ, Lei D, Liu WM, Wang ZM (2020) Large-scale shaking table model test on seismic performance of bridge-pile-foundation slope with anti-sliding piles: a case study. *Bull Eng Geol Env* 79:1429–1447
- Zhu CQ, Huang Y, Sun J (2020) Solid-like and liquid-like granular flows on inclined surfaces under vibration-Implications for earthquake-induced landslides. *Comput Geotech* 123:103598
- Zhu CQ, Cheng HL, Bao YJ, Chen ZY, Huang Y (2022) Shaking table tests on the seismic response of slopes to near-fault ground motion. *Geomech Eng* 29(2):133–143